

Modeling of the outer electron belt during magnetic storms

L. Desorgher, P. Bühler, A. Zehnder

Paul Scherrer Institute, CH-5232 Villigen PSI

E. Daly, L. Adams

ESA/ESTEC, NL-2200 AG Noordwijk, The Netherlands

Abstract The flux dropout of relativistic electrons in the earth's outer radiation belt, during the main phase of the 26 March 1995 magnetic storm is examined. Outer belt measurements by the Radiation Environment Monitor, REM aboard the STRV-1b satellite are presented to characterize this dropout. In order to simulate the dynamics of the electron belt during the storm main phase a particle tracing code was developed which allows to trace the trajectories of electrons in a dynamic magnetospheric electromagnetic field. Two simulations were performed in a non-stationary magnetic field, one taking only the induced electric field into account (fully adiabatic motion), and one with an additional non-stationary convection electric field. The simulations show, that adiabatic deceleration can produce the observed count rate decrease and also the observed inward motion of the count rate peak.

The convection electric field causes diffusion, which can take particles from low L values out to the magnetopause and contribute to an additional loss of particles, which is suggested by the observations.

1. Introduction

During magnetic storms drastic changes of the relativistic electron population, trapped in the earth outer radiation belt are observed [Baker et al., 1986]. During the storm main phase, typically a decrease of the electron flux by up to a few orders of magnitude is observed, which during the recovery phase is followed by an increase. The peak flux measured after the storm is often higher than the prestorm level.

A mechanism invoked to explain the dropout during the main phase of a storm is adiabatic deceleration of the particles due to the ring current induced magnetic field changes [Mc Ilwain, 1996]. The main phase of a storm is characterized by the growth of the ring current and an associated decrease of the magnetic field strength in the inner magnetosphere. If all three adiabatic invariants are assumed to be conserved, the trapped particles move outward and are decelerated in the decreasing magnetic field, which can lead to a decrease of the measured flux.

However, observations [Li et al., 1997] suggest that real losses of relativistic electrons from the trapping region happen as well. This loss of particles is still not fully explained. Different studies show that precipitation of particles into the atmosphere is not the dominant loss process. Another possible loss could be projection of electrons into the magnetopause due to the magnetic field variation induced outward movement of the trapped particles.

In this paper we study the dropout of the relativistic electrons observed during the 26 March 1995 storm with the Radiation Environment Monitor, REM aboard the UK satellite STRV-1b. We developed a single particle code, for tracing the guiding center motion of charged particles in a non-stationary geomagnetic field. Using magnetic field models, which have included the effects of the ring current, the adiabatic deceleration and the radial movement of particles are investigated. In a first section the measured electron fluxes are presented together with the Dst index and the solar wind pressure P_{sw} deduced from the SWE experiment on the WIND satellite. In the following the magnetic and electric field models used to simulate this particular storm are described and results of the particle tracing calculations, are presented. Finally the calculations are compared with the observations and the results are discussed.

2. Observations

To study the outer electron belt variation during the 26 March 95 storm, we use measurements of the relativistic electrons from the Radiation Environment Monitor, REM [Bühler et al., 1996]

onboard the UK satellite STRV-1b [Wells, 1994]. STRV-1b was launched on 17 June 1994 into a Geostationary Transfer Orbit with an inclination of 7° and a period of ~ 10.5 h. STRV-1b passes two times per orbit through the radiation belts, covers the L-range from 1.1 to $7.0 R_E$ and thus provides an ideal platform to study electron belt dynamics.

The REM data for the period from 25 to 29 March 1998 is plotted in figure 1 (uppermost panels) together with the Dst index (middle panel) and solar wind dynamic pressure deduced from the SWE experiment aboard the WIND spacecraft [Ogilvie et al., 1995].

The count rates measured by REM are plotted versus L for different crossings of the outer belt. The values of McIlwain's L-shell parameter [McIlwain, 1966] used throughout this paper were computed with IGRF95 internal [Langel, 1992] and Tsyganenko89 external geomagnetic field models [Tsyganenko, 1989] with $K_p=0$. The left panel shows crossings before and during the storm main phase, the right one shows crossings during the recovery phase. The curves are gathered into five groups referred to by letters (a), (b), (c), (d), and (e), which are also reproduced on the Dst plot to indicate at which periods of the storm (bold sections of Dst curve) the count rates have been measured. Note, that the curve (c) is reproduced in both, the left and right panel, in order to facilitate comparison.

The 26 March 1995 magnetic storm resulted from the interaction of a corotating interaction region, CIR [Tsurutani et al., 1995] with the magnetosphere. A sudden storm commencement (Dst increase) occurred on 26 March from 00 UT to 04 UT. It is the signature of the compression of the magnetosphere by the solar wind dynamic pressure increase.

During the main phase of the storm, which lasted from 04 UT to 18 UT on 26 March, Dst decreased to -100 nT due to the injection of particles into the ring current. At the beginning of the recovery phase, Dst first steeply increased (from 18 UT on 26 March to 04 UT on 27 March) presumably due to the rapid decay of the ion population in the ring current, and then went over into a slow recovery phase.

The left top panel shows that before the storm the electron flux in the outer radiation belt was high, but rather stable. During the main phase the count rates decreased over the whole L range, to reach around 18 UT on 26 March a minimum, represented by curve (c). The factor between the maxima in curves (a) and (c) is about 50. Note, that the L value at which the flux is maximum apparently moved inward.

The dropout of the count rate correlates with the decrease of Dst and so with a decrease of the

magnetic field strength in the relevant part of the magnetosphere. The mechanism usually invoked to explain this observation is adiabatic deceleration [Mc Ilwain, 1996]. If the three adiabatic invariants are conserved a decrease of the magnetic field induces a deceleration and an outward motion of the particles. As the particles are decelerated the flux at a fixed energy and thus the count rates in a fixed threshold detector decrease. Since this process is reversible the outer belt should return to its precedent state as Dst recovers. The upper right panel shows that during the beginning of the recovery phase, when Dst significantly increased, the count rates also increased over the whole L range (curve (c) to curve (d)). This is in agreement with the adiabatic theory. But during the rest of the storm (curve (d) and (e)), whereas below L=4 the count rates remained nearly constant, they significantly increased above L=4.

We argue that below L=4 the count rates are dominated by the remanent part of the electron population before the storm and above L=4 a new population appeared, which was brought into the inner magnetosphere by injection or by an acceleration processes distinct from adiabatic acceleration [Li et al., 1996]. Comparing the remanent part of the belt in curve (d) with curve (b), where Dst is about on the same level we note that this part does not fully recover to its prestorm value. This indicates that non-adiabatic processes or losses occur during the main phase. A conceivable mechanism is pitch angle scattering into the loss cone and subsequent absorption in the atmosphere. However, two studies [Imhof et al., 1991; Li et al., 1996] have shown that this is not the dominant loss process for relativistic electrons during magnetic storms.

Another possible loss mechanism is the projection of electrons into the magnetopause, which we attempt to investigate with our simulations.

3. Simulations

3.1. Field models

We simulated the variation of the magnetosphere during the 26 March storm by using non-stationary magnetic and electric field models.

The magnetic field is symmetric about the equatorial plane and the azimuthal angle, and is given by the sum of a static dipole field B_{dip} and a variable ring current field \vec{B}_{RC} , which in cylindrical coordinates (ρ, φ, z) is given by

$$\vec{B}_{RC}(\vec{r}, t) = STR_{RC}(Dst, P_{sw}) \cdot \vec{B}_1(\rho, z) \quad (1)$$

The strength of the ring current STR_{RC} is defined by the following function of solar wind pressure and Dst index [Olson and Pfitzer, 1982]

$$RC_{STR}(Dst, P_{sw}) = -0.03Dst + .9546\sqrt{P_{sw}} + 0.45 \quad (2)$$

The variation of STR_{RC} during the 26 March storm is plotted in figure 2a). It mainly follows the variation of Dst. The stationary field $\vec{B}_1(\rho, z)$ is the curl of an azimuthally symmetric vector potential defined by

$$A_{1,\varphi} = \sum_{i=1}^7 \frac{4B_i\rho_i^3\rho}{(\rho^2 + z^2 + 4\rho_i^2)^{3/2}} \quad (3)$$

A sum of two similar terms, which was introduced by Tsyganenko [1987] to model the ring current field, was used by Hilmer and Voigt [1995] for the Hilmer-Voigt 95 magnetic field model. In the presented case the values $\rho_i=0.5,1.0,2.0,3.0,4.0,5.0,6.0 R_E$ and $B_i=-7.75, 12.51, -148.00, 888.25, -1654.19, 1231.09, -349.42$ nT, were used. These parameter values were selected to approximate the equatorial radial profile of the Olson-Pfitzer ring current field at midnight. The resulting radial profile of B_1 is plotted in figure 2b).

The magnetic field variation induces an electric field given by

$$E_\varphi = -\frac{\partial STR_{RC}}{\partial t} A_{1,\varphi} \quad (4)$$

In a first simulation we just considered this induced electric field, which permits to study the effect of the ring field current on the outer electron belt. In a second simulation the corotation electric field and a non-stationary convection field were added. The convection electric field was modeled by the gradient of a scalar potential

$$\varphi_{conv} = \frac{50kV}{2} \left(\frac{R_{eq}}{8.547}\right)^2 \sin\varphi + \frac{\Delta V(t)}{2} \frac{R_{eq}}{8.547} \sin\varphi \quad (5)$$

where R_{eq} expressed in R_E is defined by the distance between the earth center and the the point where the magnetic field line crosses the equatorial plane.

The quiet time convection electric field is modeled by the first term in equation (5), corresponding to a shielded Volland-Stern potential [Volland, 1973, Stern, 1974]. The variation of the convection electric field (second term in equation (5)) is simulated by a non-shielded Volland-Stern potential.

The amplitude $\Delta V(t)$ is formed by a series of peaks which suddenly increase and then decrease exponentially in about 20 minutes. These peaks represent the different substorms occurring during the storm. This variable convection electric field model was used by Chen et al. [1994] to study the injection of ring current particles during magnetic storms. In our model $\Delta V(t)$ is non-zero during the storm main phase from 07 UT to 21 UT on 26 March and vanishes before and after this period. In figure 2 c) the variation of the uniform dawn-dusk convection electric field derived from $\Delta V(t)$ is plotted versus time.

3.2. Particle trajectories

In order to compute particle trajectories the relativistic guiding center equation

$$\frac{d\vec{R}}{dt} = \frac{\vec{B}}{B^2}(-\vec{E} + \frac{M}{q\gamma}\nabla B) \quad (6)$$

is solved in the electromagnetic fields described above. $M = \frac{p^2}{2m_0B}$ is the first adiabatic invariant, q is the charge of the particle and γ is the well known relativistic factor. In all calculations M is assumed to be conserved.

For the simulation without convection electric field the magneto-electric field model is azimuthally symmetric which makes the third adiabatic invariant to be conserved. Results of this first simulation are shown in figure 3. In the middle panel the radial distance from the center of the earth of electrons starting before the storm at different $r_0 = 3, 4, 5, 6 R_E$ is plotted versus time.

The lower panel shows the energy variation of the same electrons assuming a start energy of 1 MeV. For comparison the Dst index is plotted for the same period in the top panel. Since the first and the third invariants are conserved, the electrons move outward and are decelerated when Dst decreases, and move inward and are accelerated when Dst increases. Even if the model is a simple approximation of the real magnetosphere the fact that electrons starting at $6 R_E$ reach $10 R_E$ shows that during the main phase of important storms it must be considered that particles can be lost into the magnetopause.

The energy variation is important. Since the electron spectrum is a falling function with increasing energy, deceleration leads to a decrease of the flux at a given energy.

Adding the convection electric field the model is no more azimuthally symmetric and the motion of particles depends also on the azimuthal angle. The third adiabatic invariant is no longer conserved.

Figure 4 shows results of trajectory computations for the case with a convection electric field. The different lines represent the radial motion of electrons starting at a radius of $r_0=4 R_E$, with an energy of 1 MeV at different local times (noon, midnight, dawn, dusk). The bold line represent the motion of a particle without convection electric field. Before and after this period, the non-stationary term of the convection electric field is zero, the third adiabatic invariant is conserved, and the electron motion is the same as in the the first simulation.

In this particular case the electrons starting in the midnight and dawn sector are lost into the dayside magnetopause, whereas the electrons starting at noon and dusk stay in the magnetosphere. The electron starting at noon is at the end of electric field variations even below the curve which represents adiabatic motion. Whether a particle finally experiences an overall in- or outward force depends on where it is located in local time, during periods when the electric field is strong. As the resulting electric force is always from dusk to dawn, particles at dusk are accelerated inward and particles at dawn, outward. The convection electric field is the source of radial diffusion. Together with the adiabatic outward motion during the main phase of the storm, this diffusion leads to loss of outer belts electrons in the dayside magnetopause even for particles starting at $4 R_E$.

3.3. Flux variation

An iterative algorithm was applied to compute the evolution of the electron flux $j(r, \varphi, E, t)$ in time. The starting point were the REM measurements from 24/25 March. From these measurements $j_0(r, \varphi, E, t_0)$ was deduced, which was approximated by

$$j_0(r, E, t_0) = f(L) \cdot \exp(-\alpha(L) \cdot E) \quad (7)$$

and was assumed to be independent of φ .

Together with the particle tracing code and j_0 , Liouville's theorem

$$\frac{j(r_1, \varphi_1, E_1, t_1)}{B(r_1, t_1)} = \frac{j(r_0, \varphi_0, E_0, t_0)}{B(r_0, t_0)} \quad (8)$$

allows to calculate j at given time t_1 . In fact for the simulation with convection electric field this procedure was used in an iterative manner. For a given r_1 , the flux was calculated at t_0+20' for a number of azimuthal angles φ_i . The resulting spectra were averaged to give the φ independent $j_1(r_1, E, t_1) = \sum_i^n \frac{j(r_1, E, \varphi_i, t_1)}{n}$. This j_1 was then used to calculate the flux at $t_1 + 20'$ in the same

manner, and so on. Thus the method finally delivers φ independent fluxes for every 20 minutes. In order to compare the simulated fluxes with the count rates from REM, the calculated spectra were folded with the geometric factors of the detector which gives the count rates REM would measure in the presence of the simulated spectra.

In figure 4 the predicted count rates are compared with the measured rates for four different passages of the outer belt.

The top left panel corresponds to the last passage of the series (a) in the figure 1. The upper right, lower left, and lower right plots, correspond to curves (b), (c) and (d) in figure 1.

In each plot the full line represents the observations, the long dashed line the simulation without convection electric field and the short dashed lines, the simulation with convection electric field. The arrows in the upper right corner of each panel indicate in- or outbound passages.

Let us first discuss the count rates obtained with the simulation using the model without convection electric field. The count rates correspond well at the beginning of the main phase (a), showing that the applied j_0 fits the initial flux distribution. In the middle of the main phase (b) the simulated count rates closely fit the observations at $L < 4$, whereas at $L > 4$ the simulation gives count rates which are above the observations. Similar to the observations, the simulated count rates continue to decrease to reach a minimum at the end of the main phase (c), which however are lower than the observations by up to a factor 10. Comparing curves (a) and (c) it can be noted that similar to the REM data the count rate peak of the simulated flux distribution has moved inward.

If we consider that the particles move outward during the main phase we would expect the peak to move outward as well. But as the energy variation and radial movement are more important at higher L values the apparent peak moves inward. In summary we note that our simple first model can produce a decrease of the count rates even larger than observed, and also reproduce the inward motion of the peak. This illustrates that adiabatic deceleration of the particles must be considered as a major mechanism to explain flux dropouts in the outer belt.

After the rapid increase of Dst at the beginning of the recovery phase the simulated rates are close to the observations below $L=3.5$, but at higher L values the simulated count rates are significantly higher than the observations. This shows again that at least at higher L-values additional losses must occur.

We have shown in the previous section that adding the variable convection electric field can lead together with the adiabatic outward motion to a loss of particles into the magnetopause. Thus it

could be expected that the effect of a convection electric field would improve the situation. And although the flux profiles obtained with the simulations including the convection electric field do not well agree with the observations it can be noted, that the effect of the convection electric field can indeed alter the particle flux at large L values. However, with the applied field the inward diffusion is much too strong, which leads at lower L values to a flux enhancement which is not observed.

The results of such simulations depend on several parameters. Crucial are the initial flux distribution, the temporal and spatial variations of the electromagnetic fields. The field models which have been applied in this work have not been optimized to reproduce the observation but rather to approximate existing models which have been described in the literature. Several improvements have to be included in the models and a systematic analysis of the dependency of the results from the various parameters must be made.

4. Conclusion

We have studied the dropout of the high energetic electrons trapped in the outer belt during the 26 March 95 storm. Using a particle tracing code we simulated the expected flux variations due to the temporal variations of the magnetospheric fields during the storm main phase and compared them with observational data from REM. Two simulations were considered, one using field models without convection electric field and one including the effect of a non-stationary convection electric field.

The results of the first simulation show that adiabatic deceleration can explain the observed count rate decrease and inward motion of the count rate peak during the main phase rather well. However, the observations indicate that at high L values real losses occur. We argue that the combination of the adiabatic outward motion and the effect of a convection electric field leads to projection of particles into the magnetopause and contributes to the loss of electrons.

In the presented work we used standard models of the magnetic and electric fields. Future work will aim to improve these models. Note, that this kind of simulations can be used to test the validity of electromagnetic field models in the inner magnetosphere.

Acknowledgments

This study was supported by ESA/ESTEC/WMA Technology Research Contract 11108/94/NL/JG(SC).

References

- Baker D. N., Blake J. B., Klebesadel R. W. and Higbie P. R. (1986) Highly relativistic electrons in the Earth's magnetosphere, 1, Lifetimes and temporal history 1979-1984, *J. Geophys. Res.*, **91**, 4265-4276.
- Bühler P., Ljungfelt S., Mchedlishvili M., Schlumpf N., Zehnder A., Adams L., Daly E., and Nickson R. (1995) Radiation Environment Monitor *Nucl. Instr. Meth. Phys. Res.*, **386**, 825 .
- Chen M. W., Lyons L. R., and Schulz M. (1994) Simulations of phase space distributions of storm time proton ring current, *J. Geophys. Res.*, **99**, 5745-5759.
- Hilmer R. V., and Voigt G. H. (1995) A magnetospheric magnetic field model with flexible current systems driven by independent physical parameters *J. Geophys. Res.*, **100**, 5613-5626.
- Imhof W. L., Voss H. D., Mobilia J., Daltlowe D. W. and Gaines E. E. (1991) The precipitation of relativistic electrons near the trapping boundary, *J. Geophys. Res.*, **96**, 5619.
- Langel R. A. (1992) International Geomagnetic Reference Field: The sixth generation *J. Geomag. Geoelectr.*, **44**, 679 .
- Li X. , Baker D. N., Temerin M., Cayton T. E., Reeves E. G. D. , Christensen R. A., Blake J. B., Looper M. D., Nakamura R. and Kanekal S. G. (1997) Multisatellite observations of the outer zone electron variation during the November 3-4, 1993, magnetic storm, *J. Geophys. Res.*, **102**, 14123-14140.
- McIlwain C. E. (1966) Magnetic coordinates, *Space Science Reviews*, **5**, 585.
- McIlwain C. E. (1996) Processes acting upon outer zone electrons, *Geophysical Monograph*, **97**, eds. J.F. Lemaire, D. Heyndericks, and D.N. Baker, 15, AGU, Washington, D. C.
- Ogilvie K. W., Chorney D. J., Fitzenreiter R. J., Hunsaker F., Keller J., Lobell J., Miller G., Scudder J. D., Sittler Jr. E. C., Torbert R.B., Bodet D., Needel G., Lazarus A. J., Steinberg J. T., Tappan J. H., Mavretic A. and Gergin E. (1995) SWE, a comprehensive plasma instrument for the Wind spacecraft, *Space Sci. Rev.*, **71**, 55 .
- Olson W. P. and Pfitzer K. A. (1982) A dynamic model of the magnetospheric magnetic and electric fields for July 29, 1977, *J. Geophys. Res.*, **87**, 5943.
- Stern D. P. (1973) A study of the electric field in an open magnetospheric model, *J. Geophys. Res.*, **78**, 7292-7305.

- Tsurutani B. T., Gonzalez W. D., Gonzalez A. L. C., Tang F., Arballo J. K. and Okada M. (1995) Interplanetary origin of geomagnetic activity in the declining phase of the solar cycle, *J. Geophys. Res.*, **100**, 21717.
- Tsyganenko N. A. (1987) Global quantitative models of the geomagnetic field in the cislunar magnetosphere for different disturbance levels, *Planet. Space Sci.*, **35**, 1347-1358.
- Tsyganenko N. A. (1989) A magnetospheric field model with a warped tail current sheet, *Planet. Space Sci.*, **37**, 5.
- Volland H. (1973) A semiempirical model of large scale magnetospheric electric fields, *J. Geophys. Res.*, **78**, 171-180.
- Wells N. (1994) The Space Technology Research Vehicles STRV-1a and STRV-1b: First in-orbit results, *8th annual AIAA/Utha State University Conference on small satellites*.

Figure captions

Figure 1: Radial profiles of the REM count rates for different outer belt passages of STRV-1b, Dst and solar wind dynamic pressure. In order to indicate the time of the different count rate profiles, the labels (a), (b), (c), (d), (e) are reproduced in the Dst panel.

Figure 2: a) Temporal variation of the strength of the ring current, STR_{rc} , b) radial profile of the ring current magnetic field, c) variation of the non-stationary dawn-dusk convection electric field used for our simulations of the 26 March storm.

Figure 3: Dst (upper panel), radial motion (middle panel), and energy variation (lower panel) of 1 MeV equatorially trapped electrons for the simulation without convection electric field. The different lines represent particles starting at $r_0=3, 4, 5, 6 R_E$.

Figure 4: Radial motion of 1 MeV electrons starting at $r_0=4 R_E$ under the influence of the convection electric field shown in figure 2 c). The different lines represent the trajectories of particles starting at different local times. The bold line represents the motion without convection electric field (adiabatic motion).

Figure 5: Comparison between simulated and observed count rates during four outer belt passages of STRV-1b. The top left panel correspond to the last curve of series (a) in figure 1 (beginning of the storm). The upper right, lower left and lower right panel correspond to the curves (b) (c) and (d) of figure 1.

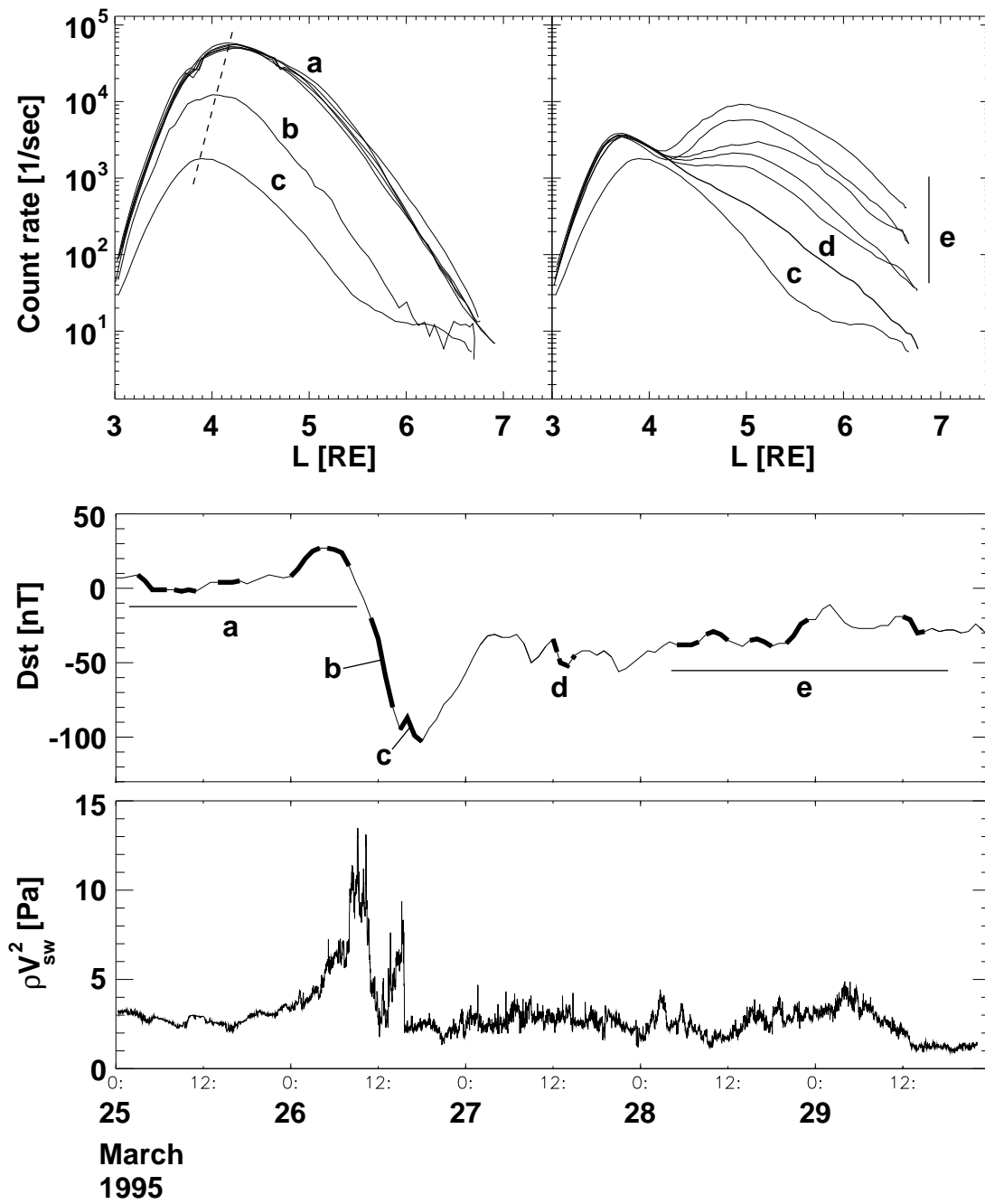


Figure 1:

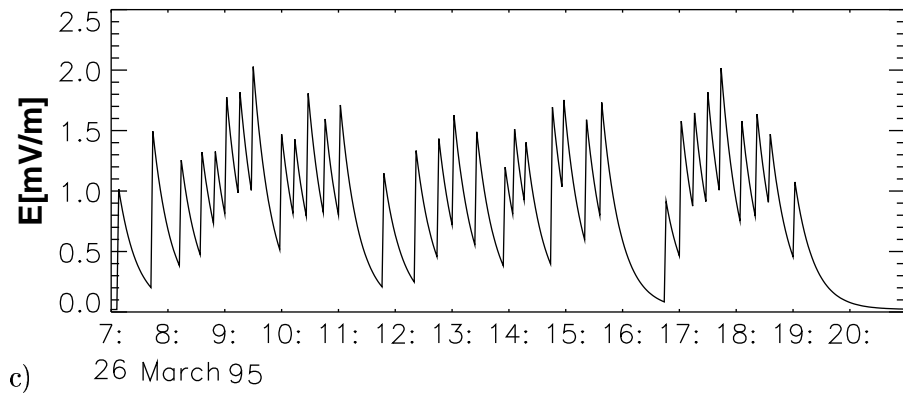
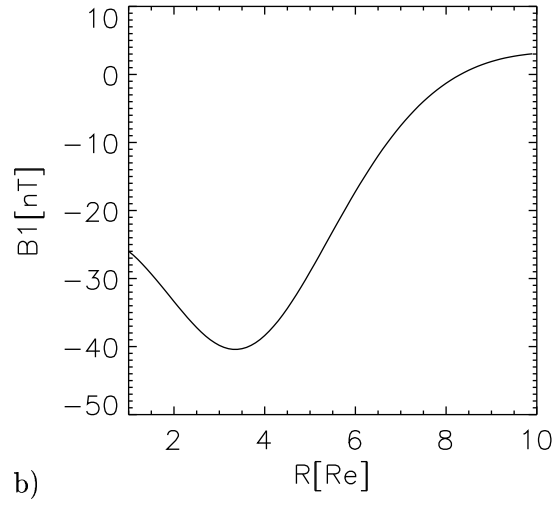
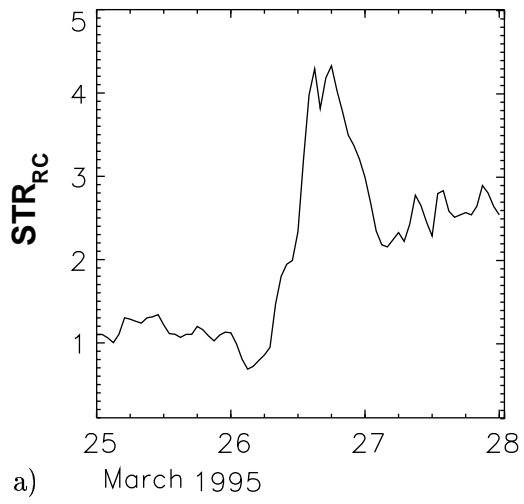


Figure 2:

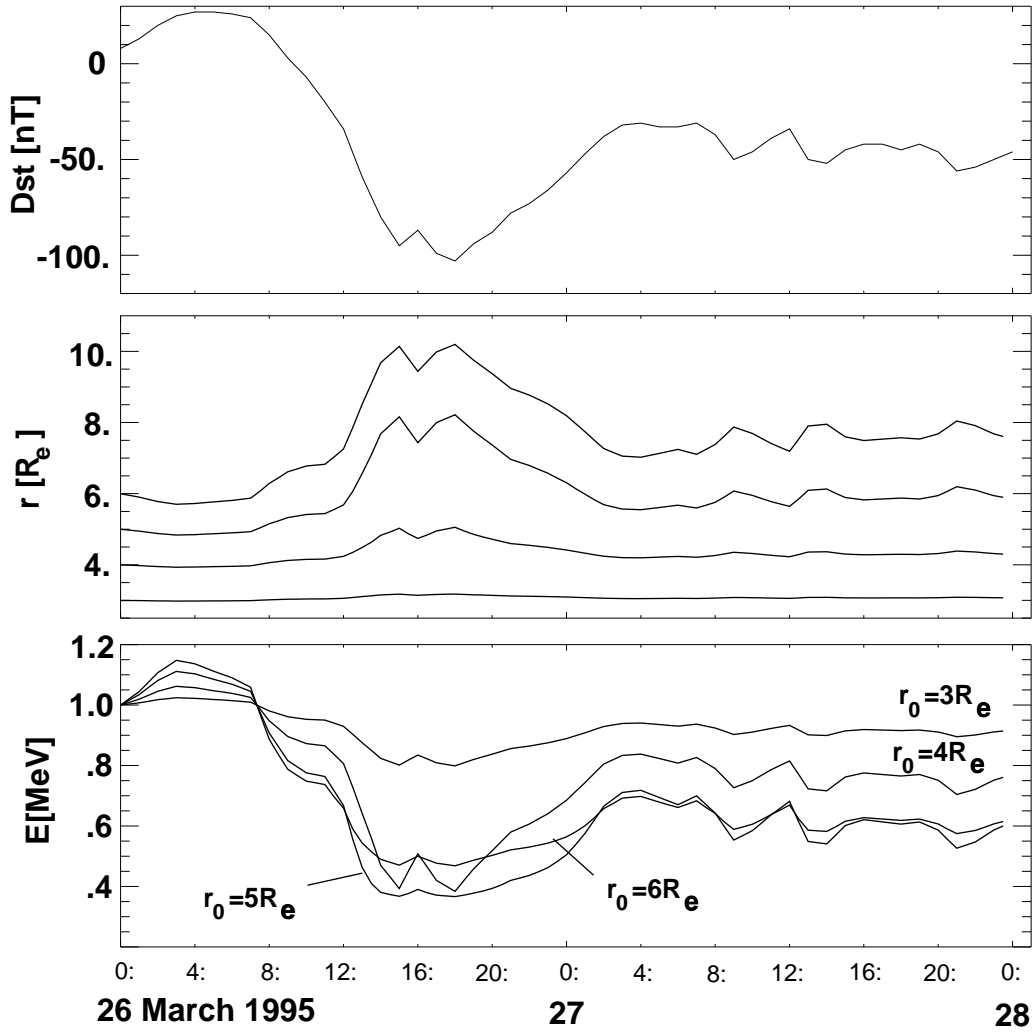


Figure 3:

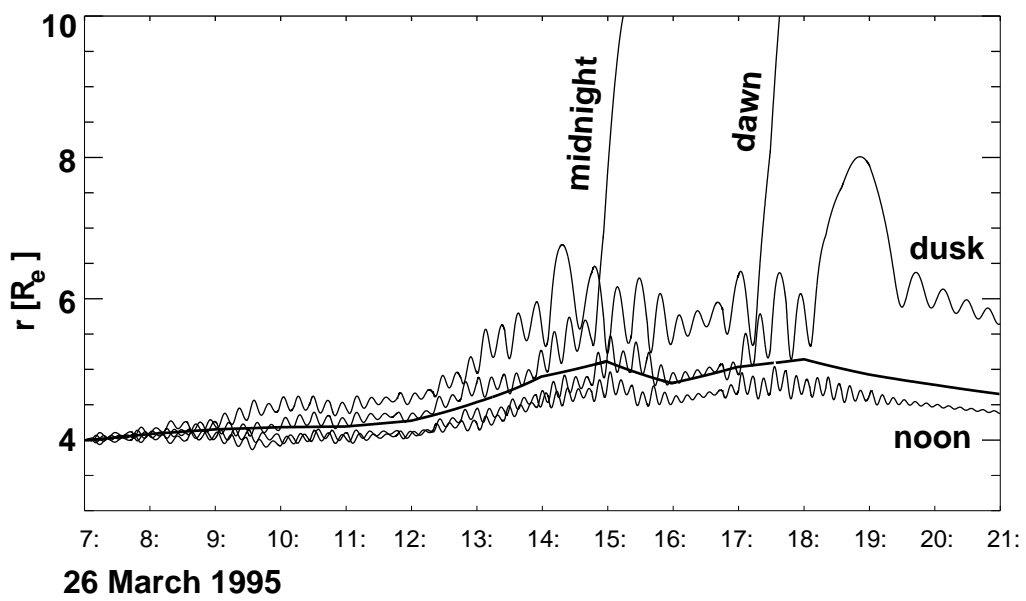


Figure 4:

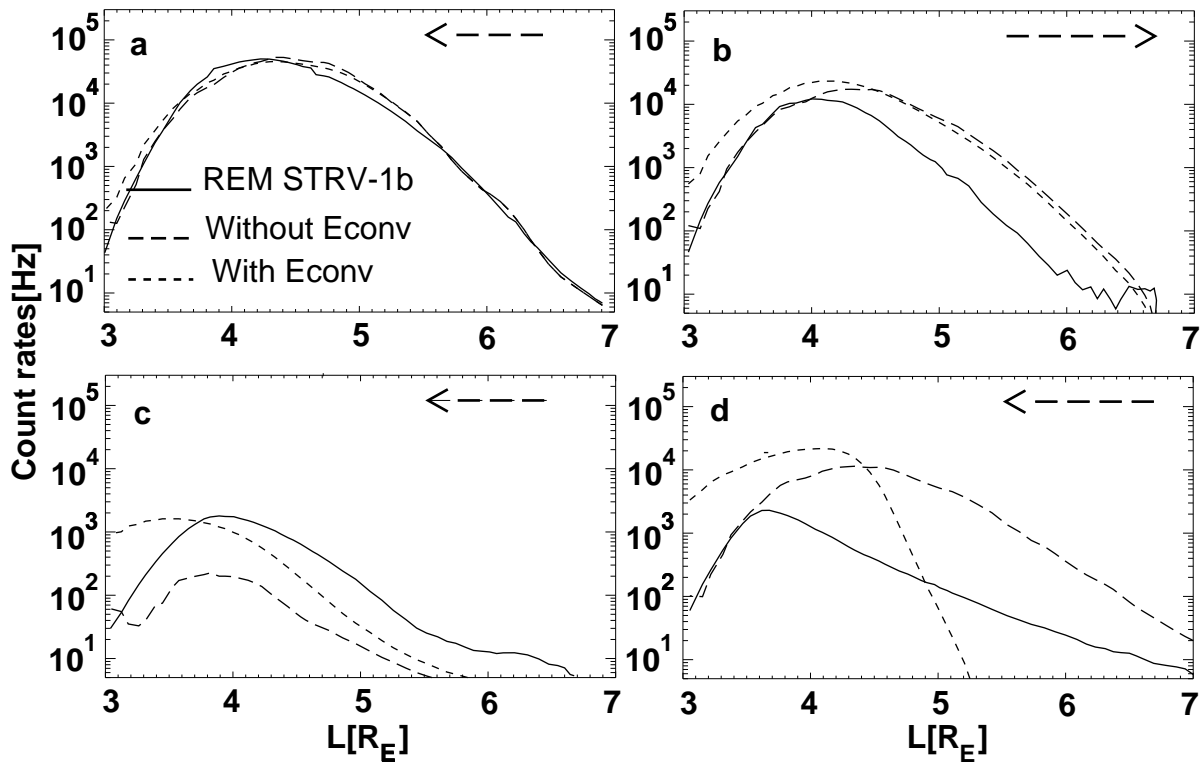


Figure 5: